

Co-existence of short- and long-range magnetic order in LaCo_2P_2

Ola Kenji Forslund,^{1,*} Daniel Andreica,² Hiroto Ohta,³ Masaki Imai,⁴
Chishiro Michioka,⁴ Kazuyoshi Yoshimura,⁴ Martin Månsson,^{1,†} and Jun Sugiyama^{5,6}

¹*Department of Applied Physics, KTH Royal Institute of Technology, SE-106 91 Stockholm, Sweden*

²*Ioan Ursu Institute, Faculty of Physics, Babes-Bolyai University, 400084 Cluj-Napoca, Romania*

³*Faculty of Science and Engineering, Doshisha University, Kyotanabe, Kyoto 610-0321, Japan*

⁴*Department of Chemistry, Graduate School of Science, Kyoto University, Kyoto 606-8502 Japan*

⁵*Neutron Science and Technology Center, Comprehensive Research*

Organization for Science and Society (CROSS), Tokai, Ibaraki 319-1106, Japan

⁶*Advanced Science Research Center, Japan Atomic Energy Agency, Tokai, Ibaraki 319-1195, Japan*

(Dated: July 8, 2021)

The ferromagnetic (FM) nature of the metallic LaCo_2P_2 was investigated with the positive muon spin rotation, relaxation and resonance ($\mu^+\text{SR}$) technique. Transverse and zero field $\mu^+\text{SR}$ measurements revealed that the compound enters a long range FM ground state at $T_C = 130.91(65)$ K, consistent with previous studies. Based on the reported FM structure, the internal magnetic field was computed at the muon sites, which were predicted with first principles calculations. The computed result agree well with the experimental data. Moreover, although LaCo_2P_2 is a paramagnet at higher temperatures $T > 160$ K, it enters a short range ordered (SRO) magnetic phase for $T_C < T \leq 160$ K. Measurements below the vicinity of T_C revealed that the SRO phase co-exists with the long range FM order at temperatures $124 \leq T \leq T_C$. Such co-existence is an intrinsic property and stems from competition between the 2D and 3D interactions/fluctuations.

I. INTRODUCTION

The interplay between magnetism and superconductivity is a long-term popular problem, particularly since the discovery of high- T_C cuprates, because the ground states are usually considered incompatible with each other [1]. While the coexistence of both phases have been reported [2, 3], a competition between the two phases is more common and has been observed in many systems such as rare earth (R) $R\text{Ni}_2\text{B}_2\text{C}$ [4], K doped $\text{Ba}_{1-x}\text{K}_x\text{Fe}_2\text{As}_2$ [5] or $\text{BaFe}_{1.89}\text{Co}_{0.11}\text{As}_2$ [3]. The latter two compounds in particular crystallize in a ThCr_2Si_2 -type structure, for which the general structure is described by AT_2X_2 with a metal A , transition metal T and metalloid X atoms. In these systems, the interactions are presumably dominated by low dimensional fluctuations within the edge-sharing TX_4 tetrahedra layers. The interlayer interaction across the A layer is heavily dependent on the $X - X$ bonding distance, which naturally changes depending on the specific elements that occupy each site of AT_2X_2 . As a result, many ground states, such as, paramagnetism (PM), ferromagnetism (FM), antiferromagnetism (AF), short range order and superconductivity have been reported for AT_2X_2 [6–9], since this family can accommodate many elements and combinations. The flexibility in the combination of constituent elements results in ground states that greatly varies with chemical doping [8–10] and by application of hydrostatic pressure [7].

It has been observed in several AT_2P_2 ($A = \text{Ca}, \text{Sr},$ and Ba , and $T = \text{Fe}, \text{Co},$ and Ni) compounds that the magnetic phase transitions are related to subtle structural

changes in the crystals [6, 11, 12]. These compounds have shown to transform from an uncollapsed tetragonal (ucT) phase to a collapsed tetragonal (cT) phase as a function of chemical doping [6, 9, 12], which naturally affects the ground state. While the majority of the AT_2P_2 compounds exhibit AF or PM ground states, LaCo_2P_2 is an itinerant FM with $T_C = 125$ K. Early magnetization measurements showed a Curie-Weiss behavior at higher temperatures above T_C [6, 13]. Neutron diffraction measurements on a polycrystalline sample revealed a collinear FM structure along the a -axis with an ordered moment of $0.44(3) \mu_B$ (Fig. 1) [14]. Indeed, a recent magnetization measurements, performed on a single crystal at low temperature, suggests a highly anisotropic FM ground state [15]. Meanwhile, the spin-lattice relaxation rate reported in a ^{31}P -NMR study [15] indicated a 3D character of the spin fluctuations above T_C .

Since LaCo_2P_2 exhibits a 3D character above T_C , but a highly anisotropic character below T_C , it is of high interest to study the crossover between these two regimes across T_C . Therefore, we have initiated a detailed of LaCo_2P_2 using muon spin rotation, relaxation and resonance ($\mu^+\text{SR}$), taking advantage of the fact that $\mu^+\text{SR}$ can offer information about the internal magnetic field distributions of both static and dynamic characters [16–18]. In this study, a cascade of magnetic transitions is observed using $\mu^+\text{SR}$. In particular, both short and long range magnetic ordered phases are likely to coexist in LaCo_2P_2 in the vicinity of T_C . Such behavior is attributed to an intrinsic property and is most likely originating from the competing interactions of different dimensionality.

* okfo@kth.se

† condmat@kth.se

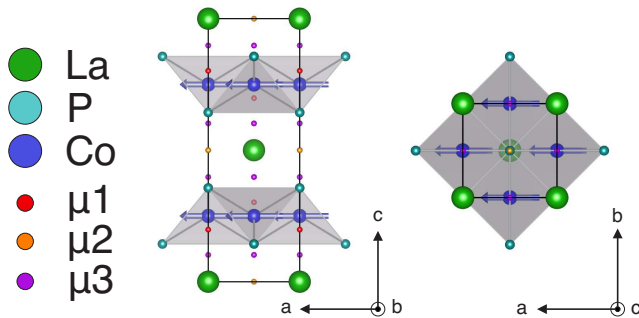


FIG. 1. The magnetic structure of LaCo_2P_2 proposed by Ref. 14. The predicted muon sites by DFT calculations are indicated as spheres: red $\mu 1$ at $(0,0,0.198)$, orange $\mu 2$ at $(0,0.5,0.102)$ and purple $\mu 3$ at $(0,0,0.5)$. The coordinates are specified for the crystal space group $I4/mmm$ (#139): $a = 3.812$, $b = 3.812$, $c = 10.984$ Å. The magnetic moments are indicated as blue arrows within the CoP-polyhedra.

II. EXPERIMENTAL SETUP

Polycrystalline LaCo_2P_2 was prepared from pure La, and Co and P starting materials. LaP and Co_2P were first synthesized by a solid state reaction between La/Co and P in evacuated quartz tubes at $800^\circ\text{C}/700^\circ\text{C}$. LaCo_2P_2 could then be synthesized from a solid state reaction between LaP and Co_2P , kept at 1000°C for 20 hours in an Ar atmosphere. Details about the sample synthesis can be found elsewhere [19, 20].

The μ^+ SR measurements were performed at the Dolly instrument at the $S\mu\text{S}$ muon source at Paul Scherrer Institute, Switzerland. A top loaded ^4He cryostat was used in order to reach temperatures down to ~ 2 K. About 500 mg of powder sample was inserted into an Al-coated Mylar tape envelope. The envelope was attached to a low-background fork type sample holder made of Cu. The μ^+ SR data was analyzed using MUSRFIT [21].

The muon sites and the local spin density at the muon sites in LaCo_2P_2 were predicted by density functional theory (DFT) calculations using a full-potential linearized augmented plane-wave method within generalized gradient approximation as implemented in WIEN2k program package [22]. In the calculations, the lattice parameters and atomic positions of LaCo_2P_2 were taken from Ref. 6. The magnetic moments were aligned parallel to the $[100]$ direction through spin-orbit coupling. The muffin tin potential radii (R_{MT}) for La, Co, and P were taken to be 2.50, 2.36, and 1.84 Å, respectively. The energy cutoff was chosen to be ($R_{\text{MT}} \times K_{\text{max}} = 7.0$, and $20 \times 20 \times 20$ k -points meshes were used in the Brillouin zone. Here, K_{max} is the maximum modulus for the reciprocal vectors.

III. RESULTS

The presentation of the μ^+ SR results of LaCo_2P_2 is divided into sections based on the type of field configuration chosen for the μ^+ SR experiments: transverse field (TF) or zero field (ZF). Transverse refers to the applied field direction with respect to the initial muon spin polarization. Additionally, the ZF time spectra collected at base temperature is reproduced based on the published magnetic structure and muon site determined from DFT calculations.

A. Transverse field

Figure 2 shows the collected TF (~ 50 Oe) spectra of LaCo_2P_2 for selected temperatures. At high temperatures, a distinct oscillation is observed with a frequency of about 0.7 MHz, corresponding to the applied field TF. As the temperature is lowered, the amplitude of the 0.7 MHz oscillation, *i.e.* the asymmetry due to the applied TF, decreases. Although, the amplitude is not completely diminished at lower temperature. Moreover, a faster oscillation can be observed in the time spectra at lower temperatures, accompanied by a positive offset. Therefore, the TF spectra were fitted using a combination of three exponentially relaxing cosine oscillations together with a non-oscillating exponential relaxation:

$$\begin{aligned}
 A_0 P_{\text{TF}}(t) = & A_{\text{TF}}^{\text{PM}} \cos(f_{\text{TF}}^{\text{PM}} 2\pi t + \phi_{\text{TF}}^{\text{PM}}) e^{-\lambda_{\text{TF}}^{\text{PM}} t} \\
 & + A_{\text{TF}}^{\text{imp}} \cos(f_{\text{TF}}^{\text{imp}} 2\pi t + \phi_{\text{TF}}^{\text{imp}}) e^{-\lambda_{\text{TF}}^{\text{imp}} t} \\
 & + A_{\text{FM}} \cos(f_{\text{FM}} 2\pi t + \phi_{\text{FM}}) e^{-\lambda_{\text{FM}} t} \\
 & + A_{\text{S}} e^{-\lambda_{\text{S}} t},
 \end{aligned} \quad (1)$$

where A_0 is the initial asymmetry determined by the detector geometry of the instrument and P_{TF} is the muon spin polarization function in TF configuration. A_{TF} , f_{TF} , ϕ_{TF} and λ_{TF} are the asymmetry, frequency, initial phase and depolarization rate resulting from the applied TF, where the superscripts PM and imp represent the contributions from the paramagnetic (PM) and impurity (imp) phases, respectively. Furthermore, A_{FM} , λ_{FM} , f_{FM} , ϕ_{FM} and λ_{FM} represent contributions from the internal FM field, together with A_{S} , λ_{S} . In particular, A_{FM} represents the internal magnetic field contributions that are perpendicular to the initial muon spin polarization, while A_{S} are contributions from the internal field that are parallel to the initial muon spin polarization.

In order to properly separate the PM and the impurity phases under the applied TF, the constraint $\phi_{\text{TF}}^{\text{PM}} = \phi_{\text{TF}}^{\text{imp}}$ was set. Since an oscillating fraction of 0.08 was obtained at 110 K well below T_{C} , the sample is found to contain about 34 % PM impurity phase, most likely Co_2P . Therefore, $A_{\text{TF}}^{\text{imp}} = 0.0843(46)$ was fixed through the whole temperature range since this fraction should be temperature independent. Finally, the total asymmetry was fixed to

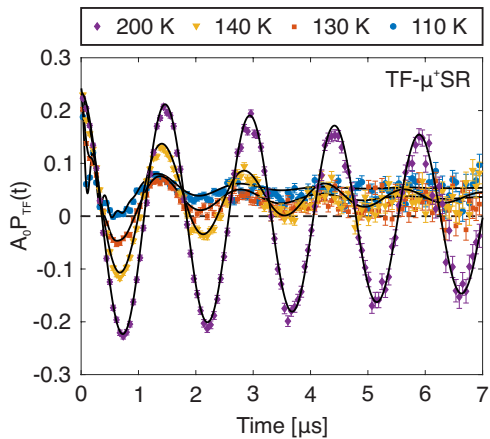


FIG. 2. Transverse field μ^+ SR spectra for selected temperatures ($T = 110, 130, 140$ and 200 K) for the LaCo_2P_2 compound. Solid lines represent the best fit using Eq. (1).

0.2351 for the measurements above 125 K, a value obtained from a high temperature measurement.

The obtained fit parameters using Eq. (1) with the procedure as described above are displayed in Fig. 3. Each asymmetry component has a temperature dependence that is expected for a magnetically ordered sample. For $T < 130$ K, $A_{\text{TF}}^{\text{PM}} = 0$ and exhibits a sharp change at a certain critical temperature. Since $A_{\text{TF}}^{\text{PM}}/(A_0 - A_{\text{TF}}^{\text{imp}})$ roughly corresponds to the PM volume fraction, the abrupt change observed at $T \approx 130$ K corresponds to the transition from a magnetically ordered state at low temperatures to magnetically disordered state at high temperatures. An accurate value of the transition temperature is obtained by fitting the $A_{\text{TF}}^{\text{PM}}(T)$ curve using a sigmoidal function, for which $T_C^{\text{TF}} = 130.17(1.18)$ K is obtained. Similarly, $A_{\text{FM}} = 0$ above T_C^{TF} while A_S poses none zero values even above T_C^{TF} , which steadily decreases with increasing temperature. Such behavior is naturally expected as these fractions stem from internal magnetic fields as described above. It should be noted that the A_S term is observed well above T_C . The origin of such behavior is underlined in the ZF section presented below.

The temperature dependencies of $\lambda_{\text{TF}}^{\text{PM}}$, $\lambda_{\text{TF}}^{\text{imp}}$ and λ_S are displayed in Fig. 3(b). $\lambda_{\text{TF}}^{\text{imp}}$ shows a steady decrease from lowest measured temperature up to the highest, and shows no anomaly at the magnetic transition. Such behaviour originate most likely from fluctuating Co d -moments and static Co and/or P nuclear moments, as also underlined in the ZF section. Such temperature dependence is similar to the one obtained in ZF configuration, underlying the quality of the fits in both field configurations. On the other hand, $\lambda_{\text{TF}}^{\text{PM}}$ is none zero only above T_C , as expected. It has a maximum just above T_C and starts to decrease with increasing temperature, reflecting an increase in the internal field dynamics. Such temperature dependence will most likely follow the

temperature dependence of magnetic susceptibility of a Curie-Weiss paramagnet. The small value of λ_{TF} (below $0.1 \mu\text{s}^{-1}$) at high temperatures suggests that the PM fluctuations eventually become motionally narrowed for the μ^+ SR time window.

The fact that $\lambda_S = 0 \mu\text{s}^{-1}$ across the whole measured temperature range suggests a static behavior of the internal FM field. Both f_{FM} and λ_{FM} represent the nature of the internal FM field but is not presented here. Instead, measurements in ZF configuration provide more accurate information regarding the internal fields. Finally, it should be noted that since $f_{\text{FM}} \sim 4$ MHz at 110 K, which is not very different from the TF precession frequency with 50 Oe (about 0.7 MHz), the estimated volume fraction of the nonmagnetic impurity phase includes an ambiguity. A more accurate value of the size of this fraction will be estimated using the ZF- μ^+ SR data.

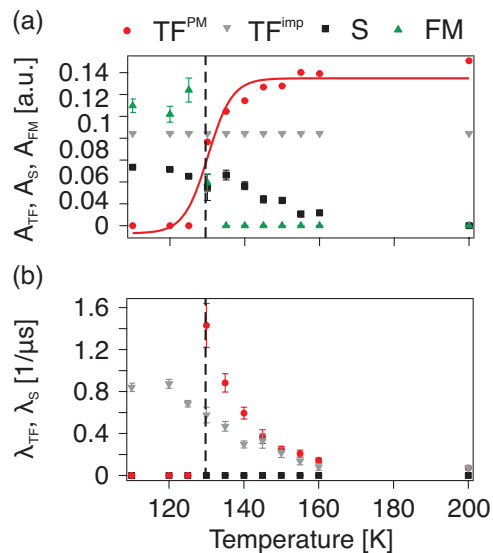


FIG. 3. Obtained fit parameters as a function of temperature using Eq. (1): (a) Asymmetry and (b) transverse field and exponential relaxation rate. The solid line in (a) is a fit using sigmoidal function. The dotted vertical line across the figure indicates the transition temperature $T_C = 130.2(1.2)$ K.

B. Zero field

ZF- μ^+ SR time spectra for selected temperatures are shown in Fig. 4. At 200 K, the ZF-spectrum in an early time domain exhibits a convex shape time dependence, which indicates a Gaussian-type relaxation. A notable small dip around $3 \mu\text{s}$ would suggest the presence of two independent Gaussian relaxations, consistent with the presence of an impurity phase. As temperature is lowered, the Gaussian relaxation is gradually changing into a more exponential like form, until an oscillation appears at lower temperatures below T_C . In order to take

into account all the phases present over the whole measured temperature range, the time spectra were fitted using a combination of two static Gaussian Kubo-Toyabe (SGKT) functions, two exponential relaxations, and one exponentially relaxing cosine oscillating terms:

$$\begin{aligned}
 A_0 P_{ZF}(t) = & A_{FM} \cos(f_{FM}2\pi t + \phi_{FM})e^{-\lambda_{FM}t} \\
 & + A_{tail}e^{-\lambda_{tail}t} \\
 & + A_F e^{-\lambda_F t} \\
 & + A_{KT}G(t, \Delta_{KT})e^{-\lambda_{KT}t} \\
 & + A_{imp}G(t, \Delta_{imp})e^{-\lambda_{imp}t}.
 \end{aligned} \quad (2)$$

A_0 is the initial asymmetry determined by the instrument's detector geometry and P_{ZF} is the muon spin polarization function in ZF configuration. The first two terms of Eq. (2), i.e., A_{FM} and A_{tail} , represents the response of the sample at low temperatures, when it enters a magnetically long range ordered state below T_C . The third and fourth terms, i.e., A_F and A_{KT} , represents the sample response above or close to T_C . The last term, A_{imp} , corresponds to the impurity phase present in the sample, a constant term throughout the whole temperature range. In detail, A_{FM} , f_{FM} , ϕ_{FM} and λ_{FM} are the asymmetry, frequency, phase, and relaxation rate resulting from perpendicular (with respect to the initial muon spin polarisation) internal field components, while A_{tail} and λ_{tail} are the asymmetry and relaxation rate of the tail component that inevitably exist in powder measurement of a magnetically ordered sample. This contribution stems from the fact that on average, 1/3 of the internal magnetic fields are parallel with respect to the initial muon spin polarisation for a perfect powder. A_F and λ_F are the asymmetry and relaxation rate of a fast component that manifests the ZF-spectra around T_C . A_{KT} and λ_{KT} correspond to the asymmetry and relaxation rate related to the static Gaussian KT, represented by $G(t, \Delta)$ where Δ is the internal field distribution width stemming from isotropically distributed magnetic moments. The same description holds also for the subscript A_{imp} signal, but corresponds to the impurity phase instead of the main phase.

In order to separate the various contributions, some constraints were set for the fits using Eq. (2). In particular, $A_{imp} = 0.0485(9)$ and $\Delta_{imp} = 0.45(2)$ were fixed across the whole temperature range, as these parameters can be expected to be temperature independent. Such values were estimated at the base temperature given that the magnetic contrast between the main and impurity phase is the biggest. Indeed, the value of Δ_{imp} suggests the presence of Co and/or P elements in the impurity phase. The value of A_{imp} corresponds to a volume fraction of 22 %, which is lower than fraction estimated from TF configuration, as expected. It is noted that measurements (not shown here) in a longitudinal field configuration i.e. field parallel with the initial muon spin polarization, at 200 K confirm that the internal fields are static, supporting the fit with two static G-KT functions and that the internal fields originate from nuclear magnetic

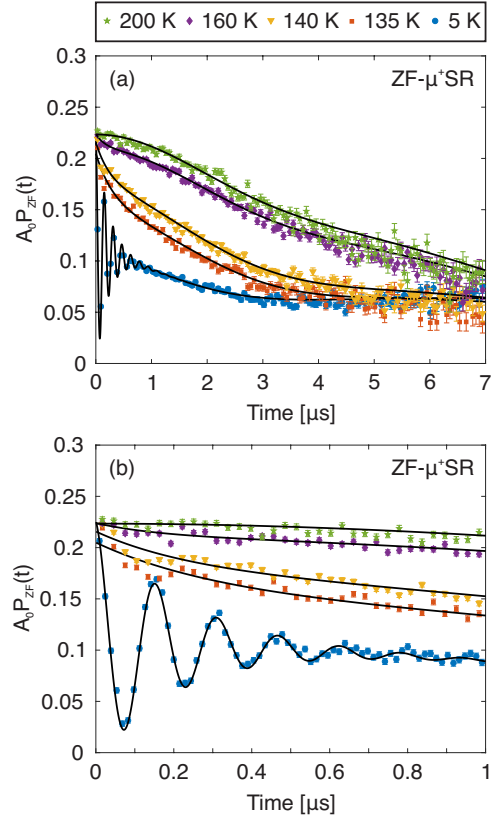


FIG. 4. Zero field μ^+ SR spectra for selected temperatures ($T = 5, 135, 140, 160$ and 200 K) for the $\text{LaCaCo}_2\text{P}_2$ compound up to (a) $7 \mu\text{s}$ and (b) $1 \mu\text{s}$. Solid lines represent the best fit using Eq. (2).

moments: $\Delta_{KT} = 0.1264(12) \mu\text{s}^{-1}$, which corresponds to $1.484237(2)$ Oe.

The temperature dependencies of the obtained fit parameters are shown in Fig. 5, using the fit procedure as described above. Below T_C^{TF} , only two asymmetry components have non zero values (except for the A_{imp} that is not shown). This is consistent with the whole main sample phase entering a long range magnetically ordered state, for which $A_{tail} \simeq \frac{1}{2}A_{FM}$. Just below T_C , a small upturn is observed in A_{tail} while a downturn is seen in A_{FM} . This is natural given that parallel fluctuations usually increases as the static perpendicular component loses its structure close to T_C . Intriguingly, the decrease of A_{FM} is followed by an additional fast relaxing component, A_F . Such component exhibits a maximum just below T_C , for which A_{FM} is still non zero, and slowly decreases with further increasing temperature. Above T_C , defined at the point where $f_{FM} = 0$ MHz and thus $A_{FM} = 0$, the spectra consist of A_{KT} and A_F components, where only A_{KT} persist above 160 K. It is noted that the fast exponential relaxation component (A_F) is present between the temperature range 124 and 160 K, i.e. across T_C . This implies that long range and short range order coexist for a narrow temperature range be-

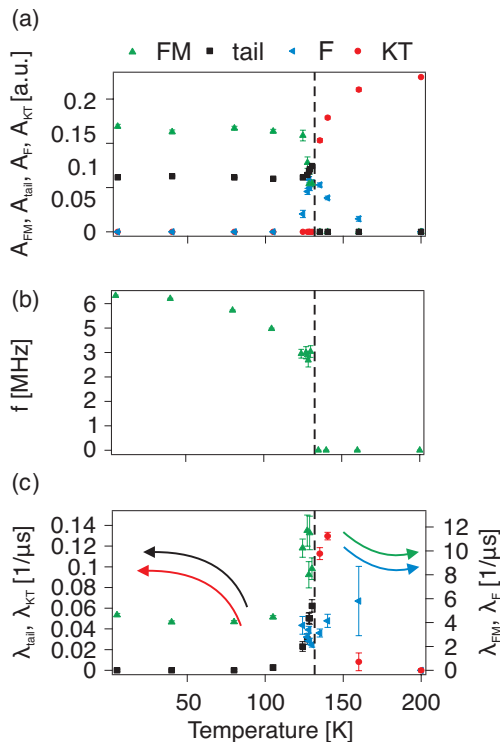


FIG. 5. Obtained fit parameters as a function of temperature using Eq. (2): (a) Asymmetry, (b) precession frequency and (c) relaxation rates. The dotted vertical line across the figure indicates the transition temperature $T_C = 130.9(7)$ K.

low T_C , which will be further discussed in Sec. IV.

The muon spin precession frequency (f_{FM}), on the other hand, exhibits an order parameter like temperature dependence. The value of the frequency corresponds to the total magnitude of the local field at the muon site. A frequency of 6.33(2) MHz is obtained at the base temperature and corresponds to 0.04670(15) T, which can be considered relatively low. Detailed calculations referencing these values are presented in Sec. III C.

As for the relaxation rates, both λ_{FM} and λ_{tail} are temperature independent at low temperatures. Here, λ_{tail} corresponds to the spin-lattice relaxation rate. The value of $\lambda_{tail}(2\text{ K}) = 0\ \mu s^{-1}$ suggests that the magnetic order at low temperatures is static. λ_{tail} increases as T_C is approached, indicating that the internal field is dynamic close to T_C . λ_{FM} on the other hand corresponds roughly to the spin-spin relaxation rate and its value can be interpreted as the field distribution width at the muon site. Similar to the λ_{tail} , an increase of λ_{FM} is observed close to T_C . Part of it can be ascribed to increase in dynamics (in principle, λ_{FM} is composed of both spin-spin and spin-lattice relaxation rates).

The temperature dependencies of λ_{KT} and λ_{imp} are consistent with the findings in TF configuration. In Eq. (2), each static Gaussian KT is multiplied by an exponential relaxation function. This is because the inter-

nal field at the muon site has two independent contributions (nuclear and electronic) and the time dependence of the muon polarization, $P(t)$, is given by the product of the expected polarization function originating from each contribution. Since the KT is the depolarization due to isotropically distributed nuclear moments, the exponential is accounting additional PM fluctuations present in the compound and it should follow the temperature dependence of λ_{TF} . Details of λ_{imp} are highlighted in Appendix A. Finally, λ_F is the additional fast relaxation rate that manifests in the time spectra close to T_C . Its temperature dependence shows a minimum close to T_C , and increases again both below and above T_C . The origin of this additional fast relaxation is discussed in Sec. IV.

C. Magnetic structure

For the sake of completeness, we have evaluated the internal field based on the FM structure proposed in Ref. 14. The magnetic structure was inferred from a combination of single crystal magnetization and polycrystal neutron diffraction (ND) measurements. In detail, ND measurements determined the $\mu_{ord} = 0.44(3)\ \mu_B$ to be aligned perpendicular to [001], which naturally cannot be resolved for tetragonal structures for a powder sample. Complementary magnetisation measurements determined then that the easy axis of magnetization to be along [100].

The expected muon sites for the given electrostatic potential and the corresponding local spin density (based on the FM structure as described above) was predicted within the Wien2K framework [22]. These calculations yield three possible muon sites; $\mu_1 = (0, 0, 0.198)$, $\mu_2 = (0, 0.5, 0.102)$ and $\mu_3 = (0, 0, 0.5)$. The complete magnetic structure together with the predicted muon sites are shown in Fig. 1 and the calculated local spin density at these sites are listed in Table I.

With this in mind, we attempt to calculate the local field at the predicted muon sites, based on the magnetic structure presented above. For a non-magnetized FM in ZF, the internal field at the muon site (\mathbf{B}_{loc}) is given by the following three components,

$$\mathbf{B}_{loc} = \mathbf{B}_{dip'} + \mathbf{B}_L + \mathbf{B}_{hf} \quad (3)$$

where $\mathbf{B}_{dip'}$ is the resulting dipole field within the considered Lorentz sphere, \mathbf{B}_L is the Lorentz field, and \mathbf{H}_{hf} is the hyperfine contact field. Such internal fields can be translated into the corresponding precession frequency via $f = (\gamma_\mu/2\pi)|\mathbf{B}|$, so that

$$f_{loc} = \frac{\gamma_\mu}{2\pi} |\mathbf{B}_{dip'} + \mathbf{B}_L + \mathbf{B}_{hf}| \quad (4)$$

where f_{loc} is the muon spin Larmor precession frequency around the internal field at the considered muon site. The

modules of Eq. 4 corresponds to the fact that μ^+ SR only detects the total magnitude of the local internal field.

In general, the local field components presented in Eq. 3 can be considered as contributions from localized and delocalized electrons. The hyperfine contact field accounts for delocalized electrons present at the muon site: *i.e.* the local spin density at the muon site. The microscopic form of such interactions requires the detailed wave function of the electron. It is however common to assume that \mathbf{B}_{hf} is isotropic, *i.e.* assuming a spherical electron wave functions. In this case, the \mathbf{B}_{hf} is simplified to

$$\mathbf{B}_{\text{hf}} = \frac{2\mu_0}{3} |\psi(\mathbf{r}_\mu)|^2 \mathbf{m}_e = \frac{2\mu_0}{3} \frac{\rho(\mathbf{r}_\mu)}{|\mathbf{m}_e|} \mathbf{m}_e, \quad (5)$$

where μ_0 is the vacuum permeability ($= 4\pi \times 10^{-7}$ H/m) and the probability density for a spherical cloud at the muon site is given by $|\psi(\mathbf{r}_\mu)|^2$, which in turn is related to the local spin density $\rho(\mathbf{r}_\mu)$. In other words, \mathbf{B}_{hf} is given as a scalar coupling between $\rho(\mathbf{r}_\mu)$ and the magnetic moment of the electron $\mathbf{m}_e = g\mu_B \mathbf{J}$ where \mathbf{J} is the total angular momentum.

The dipole field at the muon site on the other hand is originating from the dipolar interactions between localized electrons and the muon spin. A good approximation is to simply consider classical dipoles originating from spin polarized electron orbitals at the center of the magnetic atoms within a large sphere (the Lorentz sphere) with N atoms:

$$\mathbf{B}_{\text{dip}'} = \frac{\mu_0}{4\pi} \sum_j^N \frac{3\mathbf{r}_{\mu j}(\mathbf{m}_{e,j} \cdot \mathbf{r}_{\mu j})}{r_{\mu j}^5} - \frac{\mathbf{m}_{e,j}}{r_{\mu j}^3}, \quad (6)$$

where if $N \rightarrow \infty$ then $\mathbf{B}_{\text{dip}'} = \mathbf{B}_{\text{dip}}$. $\mathbf{r}_{\mu,j}$ is the distance between the muon and the j -th ion. Since the summation in Eq. (6) is not infinite but is instead limited up to within the so called Lorentz sphere, an additional contribution is added to the local field, known as the Lorentz field

$$\mathbf{B}_L = \frac{\mu_0}{3} M_L = \frac{\mu_0}{3V} \sum_j^N \mathbf{m}_{e,j} \quad (7)$$

where M_L is the vector sum of the magnetic moments inside the Lorentz sphere divided by its volume.

Based on presented theoretical models and the determined magnetic structure, the local fields were computed for the muon sites; (0,0,0.198), (0,0.5,0.102) and (0,0,0.5). The calculations were performed using Python package *MUESR* [23], and the obtained local field values are presented in Table I. Among the considered muon sites, μ_2 agrees well with the experimentally obtained data with $f_{\text{loc}} = 8.61 \simeq 6.332(23) = f_{\text{FM}}(5 \text{ K})$, although the calculated value slightly overestimates the local field in comparison to the data. This is most likely due to local

magnetic excitations present in a FM, according to the Bloch-3/2 law [24, 25], effectively lowers the precession frequency due to the spontaneous magnetization.

The Lorentz field is independent on muon site, since the considered Lorentz sphere was kept constant for the all muon sites. It is however noted that given the symmetry of the positions of μ_2 and μ_3 , $\mathbf{B}_{\text{dip}'}$ and \mathbf{B}_L are effectively canceling each other resulting into a low precession frequencies, especially for μ_3 . The hyperfine contact fields are fairly constant across the considered muon sites and constitute a fairly large portion of the resultant local field. Such behavior is different from the *A*-type AF NaNiO_2 [26], where the local field was found to be solely formed by dipolar fields. This is to some degree expected since the local spin density should be more considerable in a FM, compared to an AF.

IV. DISCUSSION

The value of the local field at the μ_2 site at low temperatures is reasonably explained by the magnetic structure determined by neutron diffraction. Therefore, we will to focus our discussion on the behavior of the compound at higher temperatures. The ZF scan presented above reveals that the sample undergoes a cascade of magnetic transitions (Fig. 6). In detail, a PM order is established at higher temperatures $T > 160$ K, as evidenced by the exponentially relaxing KT (A_{KT}). A short range order is stabilized in the temperature range $T_C < T \leq 160$ K, for which the muon spin depolarization is made up of two separate exponential relaxations (A_{F} and A_{KT} with $\Delta = 0 \mu\text{s}^{-1}$). Intriguingly, such short range order (SRO) is likely to coexist with the FM long range order (FM-LRO) in the range $124 \text{ K} \leq T \leq T_C$, for which FM-LRO is fully formed below $T < 124$ K. Such assertion is supported by the fact that A_{F} is split into two components at T_C . While A_{KT} settles to a value $\sim A_0/3$, consistent with the tail component, A_{F} shows a maximum at T_C which is separated into A_{FM} and A_{F} just below T_C . Since A_{FM} is the oscillating fraction, this is the long range ordered fraction of the sample. A_{F} on the other hand is still an exponential relaxation even below T_C , implying that there is a small temperature range in which FM-LRO and SRO co-exist.

While it was not clearly commented on, a similar behavior was observed in ^{31}P -NMR study in the raw data figure [15]. In fact, the spin-spin relaxation rate ($1/T_2$) seems to decrease between 130 and 120 K, the $1/T_2$ increases again around 110 K. Such behavior is reflected by the behavior of λ_{F} , presented in Fig. 5(c). Although NMR does not provide the information on the volume fraction, our study clearly show that a small fraction of SRO is present while the majority of the sample forms LRO.

A coexistence of LRO and SRO has been reported for SrEr_2O_4 [27] or $\text{La}_{0.7}\text{Sr}_{0.3}\text{Mn}_{1-x}\text{Co}_x\text{O}_3$ [28]. SrEr_2O_4 is a frustrated magnet where the coexistence was attributed

TABLE I. The calculated local field values at the predicted muon sites are tabulated together with the obtained local spin density $\rho(r_\mu)$ for the given magnetic structure. f_{loc} was evaluated using Eq. (4), whereas the dipole field, Lorenz field and the hyperfine contact field are given by Eq. (6), Eq. (7) and Eq. (5), respectively. The experimentally obtained precession frequency $f_{\text{FM}}(5 \text{ K})$ and the expected internal field distribution width are listed as well.

Muon site	$\rho(r_\mu) [\mu_B \text{ \AA}^{-3}]$	$B_{\text{dip}} [\text{T}]$	$B_{\text{hf}} [\text{T}]$	$B_L [\text{T}]$	$f_{\text{loc}} [\text{MHz}]$	$f_{\text{FM}}(5 \text{ K}) [\text{MHz}]$	$\Delta_{\text{LaP}_2\text{Co}_2}^{\text{calc}} [\mu\text{s}^{-1}]$
$\mu 1 (0,0,0.198)$	-0.00237581	[0.0872,0,0]	[-0.0185,0,0]	[0.0429,0,0]	15.13	6.332(23)	0.379
$\mu 2 (0,0.5,0.102)$	-0.0015081	[-0.0947,0,0]	[-0.0117,0,0]	[0.0428,0,0]	8.61	6.332(23)	0.461
$\mu 3 (0,0,0.5)$	-0.00176282	[-0.0379,0,0]	[-0.0137,0,0]	[0.0428,0,0]	1.86	6.332(23)	0.297

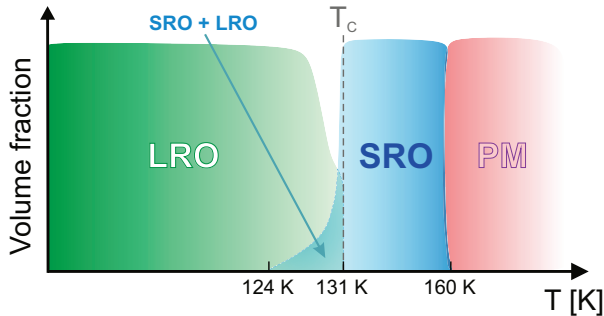


FIG. 6. Magnetic phase diagram as a function of temperature, with $T_C = 130.91(65)$. A long range magnetically ordered phase (LRO) for $T < 124$ K, a short range magnetically ordered phase (SRO) for $T_C \leq T \leq 160$ K and a paramagnetic phase (PM) for $T > 160$ K are stabilised as a function of temperature. A temperature regions in which LRO and SRO co-exist present itself for $124 \leq T \leq T_C$. The magnetic volume fractions are estimated based on Fig. 5(a).

to complex interactions arising from geometrically frustrated magnetism. For $\text{La}_{0.7}\text{Sr}_{0.3}\text{Mn}_{1-x}\text{Co}_x\text{O}_3$, on the other hand, the coexistence looks to stem from the competitions between AF and FM interactions. This would suggest that similar competitions among multiple interactions should be present in LaCo_2P_2 as well. In fact, LaCo_2P_2 shows a strong anisotropic character in the FM state, because of the 2D interactions in the CoP plane [15]. At high temperatures, on the other hand, the fluctuation were shown to be of a 3D character [15]. In other words, there exists a small temperature range for which there is a competition between the 2D and 3D character of the interactions, resulting into the coexistence of SRO and LRO. A similar separation of ordered and disordered phases has also been reported for Cu_2IrO_3 [29] and Li_2RhO_3 [30]. Theoretical treatment of such phenomena revealed that the ground state is stabilized from competition between quantum fluctuation and frustration [31, 32].

We wish to note the fact that a relatively large impurity phase is present in the compound, which could be the origin behind the anomaly around T_C . However, the signal from the impurity phase is nicely fitted with a exponentially relaxing Gaussian KT at 2 K, and it is highly unlikely that such behaviour should evolve into an exponential like relaxation at higher temperatures. The value

of the exponential relaxation rate itself is also one order of magnitude lower than the one of λ_F (Appendix A). Moreover, μ^+ SR is sensitive to detecting magnetic volume fractions, meaning each contribution is in principle separated. We wish to stress that the XRD analysis indicated no structurally phase separations, *i.e.* the sample is chemically homogeneous. The previous study underlines the high quality of our sample [15].

V. CONCLUSIONS

Transverse and zero field (ZF) μ^+ SR measurements reveal that the sample exhibits a long range ferromagnetic (FM) ground state below $T_C = 130.91(65)$ K, consistent with previous reports. The muon sites and the corresponding local spin density, based on the already reported magnetic structure, were predicted by density functional theory. The estimated local field calculations agrees well with the presented ZF- μ^+ SR data. Intriguingly, this study reveals cascade of magnetic transitions, not observed in previous studies. In detail, a paramagnetic (PM) phase is found at higher temperatures $T > 160$ K. A short range order (SRO) is stabilized at lower temperatures, for which a coexistence of the SRO and long range FM is present for $124 \text{ K} \leq T \leq T_C$. The coexistence originates from a competition of 2D and 3D magnetic interactions and/or fluctuations, prominent at T_C , since a coexistence of magnetic phases is commonly found in compounds with competing magnetic interactions.

ACKNOWLEDGMENTS

We thank the staff of PSI for help with the μ^+ SR experiments. We also appreciate H. Nozaki, M. Harada and R. Scheuermann for their help with the μ^+ SR experiments. This research was supported by the Swedish Research Council (VR) (Dnr. 2016-06955) as well as the Swedish Foundation for Strategic Research (SSF) within the Swedish national graduate school in neutron scattering (SwedNess). J.S. acknowledge support from the Ministry of Education, Culture, Sports, Science and Technology (MEXT) of Japan, KAKENHI Grant No.23108003 and Japan Society for the Promotion Science (JSPS) KAKENHI Grant No. JP26286084, JP18H01863 and

JP20K21149. D.A. acknowledges partial financial support from the Romanian UEFISCDI project PN-III-P4-ID-PCCF2016-0112 (6/2018). H.O. acknowledge support from KAKENHI Grant No. JP20K05663. The crystal figure was drawn using VESTA [33].

Appendix A: Temperature dependence of the impurity phase

The temperature dependence of the KT relaxation rate for the impurity phase, λ_{imp} , is shown in Fig. 7. The values saturates at lower temperatures and steadily decreases with increasing temperature. As mentioned in the main text, the temperature dependence follows the one obtained in TF configuration, underlying the high quality of our fits in both field configuration. Moreover, the value itself is one order of magnitude lower than that

of λ_{F} , suggesting that the origin of the additional exponential close to T_{C} is not from the impurity but is truly an intrinsic behavior of LaCo_2P_2 .

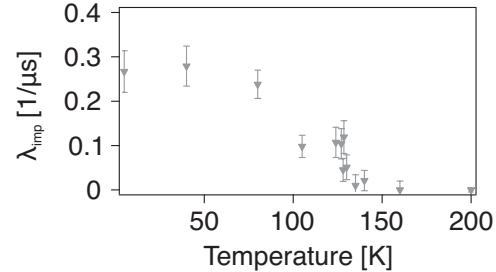


FIG. 7. Temperature dependence of the KT relaxation rate for the impurity phase

-
- [1] J. Bardeen, L. N. Cooper, and J. R. Schrieffer, *Phys. Rev.* **108**, 1175 (1957).
- [2] M. Lange, M. J. V. Bael, Y. Bruynseraede, and V. V. Moshchalkov, *Phys. Rev. Lett.* **90**, 197006 (2003).
- [3] P. Marsik, K. W. Kim, A. Dubroka, M. Rössle, V. K. Malik, L. Schulz, C. N. Wang, C. Niedermayer, A. J. Drew, M. Willis, T. Wolf, and C. Bernhard, *Phys. Rev. Lett.* **105**, 057001 (2010).
- [4] H. Eisaki, H. Takagi, R. J. Cava, B. Batlogg, J. J. Krajewski, W. F. Peck, K. Mizuhashi, J. O. Lee, and S. Uchida, *Phys. Rev. B* **50**, 647 (1994).
- [5] M. Rotter, M. Tegel, I. Schellenberg, F. M. Schapacher, R. Pöttgen, J. Deisenhofer, A. Günther, F. Schrettle, A. Loidl, and D. Johrendt, *New Journal of Physics* **11**, 025014 (2009).
- [6] M. Reehuis and W. Jeitschko, *Journal of Physics and Chemistry of Solids* **51**, 961 (1990).
- [7] R. E. Baumbach, V. A. Sidorov, X. Lu, N. J. Ghimire, F. Ronning, B. L. Scott, D. J. Williams, E. D. Bauer, and J. D. Thompson, *Phys. Rev. B* **89**, 094408 (2014).
- [8] C. M. Thompson, K. Kovnir, V. O. Garlea, E. S. Choi, H. Zhou, and M. Shatruk, *Journal of Materials Chemistry C* **2**, 7561 (2014).
- [9] J. Sugiyama, H. Nozaki, I. Umegaki, M. Harada, Y. Higuchi, K. Miwa, E. J. Ansaldo, J. H. Brewer, M. Imai, C. Michioka, K. Yoshimura, and M. Månsson, *Phys. Rev. B* **91**, 144423 (2015).
- [10] X. Tan, A. A. Yaroslavtsev, H. Cao, A. Y. Geondzhian, A. P. Menushenkov, R. V. Chernikov, L. Nataf, V. O. Garlea, and M. Shatruk, *Chemistry of Materials, Chemistry of Materials* **28**, 7459 (2016).
- [11] R. Hoffmann and C. Zheng, *The Journal of Physical Chemistry, The Journal of Physical Chemistry* **89**, 4175 (1985).
- [12] S. Jia, A. J. Williams, P. W. Stephens, and R. J. Cava, *Phys. Rev. B* **80**, 165107 (2009).
- [13] E. Mörsen, B. Mosel, W. Müller-Warmuth, M. Reehuis, and W. Jeitschko, *Journal of Physics and Chemistry of Solids* **49**, 785 (1988).
- [14] M. Reehuis, C. Ritter, R. Ballou, and W. Jeitschko, *Journal of Magnetism and Magnetic Materials* **138**, 85 (1994).
- [15] M. Imai, C. Michioka, H. Ueda, and K. Yoshimura, *Phys. Rev. B* **91**, 184414 (2015).
- [16] R. S. Hayano, Y. J. Uemura, J. Imazato, N. Nishida, T. Yamazaki, and R. Kubo, *Phys. Rev. B* **20**, 850 (1979).
- [17] O. K. Forslund, D. Andreica, Y. Sassa, H. Nozaki, I. Umegaki, E. Nocerino, V. Jonsson, O. Tjernberg, Z. Guguchia, Z. Shermadini, R. Khasanov, M. Isobe, H. Takagi, Y. Ueda, J. Sugiyama, and M. Månsson, *Scientific Reports* **9**, 1141 (2019).
- [18] J. Sugiyama, W. Higemoto, D. Andreica, O. K. Forslund, E. Nocerino, M. Månsson, Y. Sassa, R. Gupta, R. Khasanov, H. Ohta, and H. Nakamura, *Phys. Rev. B* **103**, 104418 (2021).
- [19] J. Sugiyama, H. Nozaki, M. Harada, I. Umegaki, Y. Higuchi, K. Miwa, M. Imai, C. Michioka, K. Yoshimura, E. J. Ansaldo, J. H. Brewer, D. Andreica, C. Baines, and M. Mansson, *Physics Procedia* **75**, 426 (2015), 20th International Conference on Magnetism, ICM 2015.
- [20] M. Imai, C. Michioka, H. Ohta, A. Matsuo, K. Kindo, H. Ueda, and K. Yoshimura, *Phys. Rev. B* **90**, 014407 (2014).
- [21] A. Suter and B. M. Wojek, *Phys. Proc.* **30**, 69 (2012).
- [22] P. Blaha, K. Schwarz, F. Tran, R. Laskowski, G. K. H. Madsen, and L. D. Marks, *The Journal of Chemical Physics* **152**, 074101 (2020), <https://doi.org/10.1063/1.5143061>.
- [23] P. Bonfà, I. J. Onuorah, and R. D. Renzi, “Introduction and a quick look at muon, the magnetic structure and muon embedding site refinement suite,” in *Proceedings of the 14th International Conference on Muon Spin Rotation*, <https://journals.jps.jp/doi/pdf/10.7566/JPSC.21.011052>.
- [24] S. Blundell, “Magnetism in condensed matter,” (2003).
- [25] O. K. Forslund, K. Papadopoulos, E. Nocerino, G. Morris, B. Hitti, D. Arseneau, V. Pomjakushin, N. Matsumura, J.-C. Orain, P. Svedlindh, D. Andreica, S. Jana, J. Sugiyama, M. Månsson, and Y. Sassa,

- [Phys. Rev. B **102**, 144409 \(2020\)](#).
- [26] O. K. Forslund, H. Ohta, K. Kamazawa, S. L. Stubbs, O. Ofer, M. Månsson, C. Michioka, K. Yoshimura, B. Hitti, D. Arseneau, G. D. Morris, E. J. Ansaldo, J. H. Brewer, and J. Sugiyama, [Phys. Rev. B **102**, 184412 \(2020\)](#).
- [27] T. J. Hayes, G. Balakrishnan, P. P. Deen, P. Manuel, L. C. Chapon, and O. A. Petrenko, [Phys. Rev. B **84**, 174435 \(2011\)](#).
- [28] T. D. Thanh, D. C. Linh, T. V. Manh, T. A. Ho, T.-L. Phan, and S. C. Yu, [Journal of Applied Physics, **Journal of Applied Physics** **117**, 17C101 \(2015\)](#).
- [29] E. M. Kenney, C. U. Segre, W. Lafargue-Dit-Hauret, O. I. Lebedev, M. Abramchuk, A. Berlie, S. P. Cottrell, G. Simutis, F. Bahrami, N. E. Mordvinova, G. Fabbris, J. L. McChesney, D. Haskel, X. Rocquefelte, M. J. Graf, and F. Tafti, [Phys. Rev. B **100**, 094418 \(2019\)](#).
- [30] P. Khuntia, S. Manni, F. R. Foronda, T. Lancaster, S. J. Blundell, P. Gegenwart, and M. Baenitz, [Phys. Rev. B **96**, 094432 \(2017\)](#).
- [31] M. G. Gonzalez, F. T. Lisandrini, G. G. Blesio, A. E. Trumper, C. J. Gazza, and L. O. Manuel, [Phys. Rev. Lett. **122**, 017201 \(2019\)](#).
- [32] U. F. P. Seifert and M. Vojta, [Phys. Rev. B **99**, 155156 \(2019\)](#).
- [33] K. Momma and F. Izumi, [Journal of Applied Crystallography **41**, 653 \(2008\)](#).